

Experimental evidence of the ${}^6\text{He}$ level at $E^* = 18.3$ MeV by the ${}^4\text{He}+{}^3\text{H}$ three-body reaction

O.M. Povoroznyk,* O. K. Gorpinich, O.O. Jachmenjov, H.V. Mokhnach, and O. Ponkratenko

*Institute for Nuclear Research, National Academy
of Science of Ukraine, 03680 Kiev, Ukraine*

G. Mandaglio^{1,2}, F. Curciarello^{1,2}, V. De Leo^{1,2}, G. Fazio^{1,2}, and G. Giardina^{1,2†}

¹*Dipartimento di Fisica dell'Università di Messina, 98166 Messina, Italy*

²*Istituto Nazionale di Fisica Nucleare,
Sezione di Catania, 95123 Catania, Italy*

(Dated: September 13, 2017)

Abstract

Measurements of the t-t and p-t coincidence events in the ${}^3\text{H}(\alpha, \text{ttp})$ reaction have been obtained at E_α incident energy of 67.2 MeV. Various appropriate angular configurations of detectors were chosen in order to observe the population of the ${}^6\text{He}^*$ state at around 18 MeV. Its contribution appears at the E_{tt} relative energy of 6.0 MeV by the analysis of bidimensional spectra. We found the formation of the ${}^6\text{He}$ excited state at $E^* = 18.3 \pm 0.2$ MeV (with a Γ width of 1.1 ± 0.3 MeV) by the decay into the t+t binary channel, since the threshold energy of the t+t channel is 12.31 MeV. In each analyzed bidimensional energy spectrum of (E_t, E_t) and (E_p, E_t) coincidence events resonance structures are present due to the formation of both ${}^6\text{He}^*$ and ${}^4\text{He}^*$ excited states. Our results on the E^* and Γ values regarding the ${}^6\text{He}^*$ level of about 18 MeV are compared with the results obtained by other reactions. Moreover, we also found new Γ width values of 0.7 ± 0.3 and 0.8 ± 0.4 MeV for the 14.0 ± 0.4 and 16.1 ± 0.4 MeV ${}^6\text{He}$ levels, respectively.

PACS numbers: 27.20.+n, 25.55.-e, 24.30.-v

* orestpov@kinr.kiev.ua

† ggiardina@unime.it

I. INTRODUCTION

Knowledge of the E^* energy and Γ width spectroscopic parameters of excited states of light nuclei is suitable to test the nuclear models and also to develop astrophysical studies. The best way to measure the above parameters is to study three-body reactions. In fact, the E^* and Γ values deduced by two-body scattering experiments are systematically different from the ones measured when the same states are produced by three-body reactions as two-body resonances in presence of a spectator particle. Such discrepancies are caused by a relevant background of detected particles due to other concurrent reaction channels present in the inclusive spectra (single spectra).

In a recent paper [1] using a three-body reaction we found the formation of two ${}^6\text{Li}$ states at excitation energies around 21 MeV by the decay into two ${}^3\text{He}+{}^3\text{H}$ clusters ($\tau+t$) each composed of three nucleons. This result was obtained by investigating the ${}^3\text{H}(\alpha, {}^3\text{H} {}^3\text{He})n$ kinematically complete experiment at E_α beam energy sufficient to populate the excitation energy region of our interest.

As Fig. 1 shows, the ${}^6\text{He}$ energy level distributions reported in the Ajzenberg-Selove [2] and Tilley *et al.* [3] compilations present some differences, even if we have to underline that compilation [2] appeared in 1988, compilation [3] appeared in 2002 and nowadays the results obtained by other investigated reactions have enriched the set of possible comparisons. In the diagram of ${}^6\text{He}$ levels of compilation [2] one low-lying state appears while in compilation [3] two states appear which can decay into the $\alpha+2n$ channel; moreover, above the threshold energy of 12.31 MeV for the ${}^6\text{He}^*$ states which can decay into $t+t$ clusters, compilation [2] gives only three levels up to 25 MeV of excitation energy while compilation [3] gives five levels up to 36 MeV.

Moreover, in the study of the ${}^6\text{Li}({}^7\text{Li}, {}^7\text{Be}){}^6\text{He}$ reaction [4] at incident energy of 455 MeV the ${}^6\text{He}^*$ state at $E^* = 18.0 \pm 1.0$ MeV has been observed with a Γ width of 9.5 ± 1.0 MeV by the ${}^6\text{He}^*$ decay into the $t+t$ channel, while this ${}^6\text{He}$ excited state is not present in either [2, 3] compilations. In the same work, the investigation of the ${}^6\text{Li}({}^7\text{Li}, {}^6\text{Be}){}^7\text{He}$ reaction at incident energy of 450 MeV has shown for the mirror ${}^6\text{Be}$ nucleus the analogous resonance at $E^* = 18.0 \pm 1.2$ MeV with a Γ width of 9.2 ± 1.0 MeV by the ${}^6\text{Be}^*$ decay into the $\tau+\tau$ channel. On the other hand, in the deuteron inclusive energy spectra obtained by investigation of the ${}^7\text{Li}(n,d){}^6\text{He}$ reaction [5] the ${}^6\text{He}$ states at 0.0 and 1.8 MeV of excitation

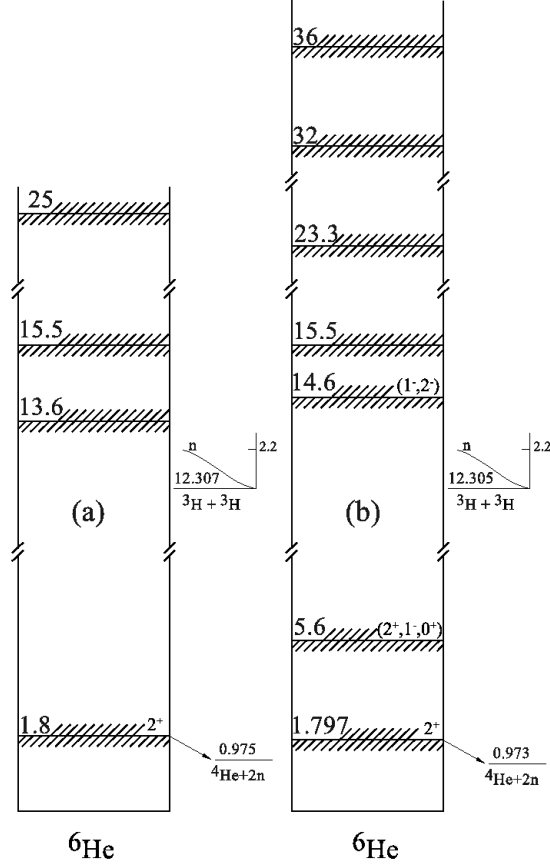


FIG. 1. Diagram of the ${}^6\text{He}$ energy levels in the Ajzenberg-Selove (a)[2] and Tilley et al. (b)[3] compilations.

energy were observed and evidence of excited states at 13.6, 15.4 and 17.7 MeV was found. Therefore, the experimental and theoretical studies on the ${}^6\text{He}^*$ level distribution are very interesting because this nucleus: i) at low excitation energies appears made of an α particle core with a halo of two neutrons, ii) at high excitation energies appears constituted of two $t+t$ clusters. Besides, the comparison between the distribution of levels for the two ${}^6\text{He}$ and ${}^6\text{Be}$ mirror nuclei is interesting.

With this state of affairs, we decided to investigate other three-body reactions such as ${}^3\text{H}(\alpha, tt)p$ and ${}^3\text{H}(\alpha, pt)t$ at E_α incident energy suitable to populate the ${}^6\text{He}^*$ levels up to around 18-19 MeV of excitation energy. By these reactions we obtained (E_t, E_t) and (E_p, E_t) bidimensional spectra useful to give information on the peak energy of ${}^6\text{He}^*$ level of our interest, also taking into account the possible contributions in the spectra of the ${}^4\text{He}^*$ states which decay into the $p+t$ channel for which the threshold energy is 19.82 MeV. In

fact, as we will explain in Sect. III, along the kinematic loci of each (E_t, E_t) or (E_p, E_t) bidimensional spectrum of the above-mentioned three-body reactions, contributions of both ${}^6\text{He}^*$ and ${}^4\text{He}^*$ state formation are present, and we have to consider that in the analysis of the t-t or p-t coincidence events.

II. EXPERIMENTAL SET-UP AND COINCIDENCE EVENT PROCEDURE

In order to study the ${}^3\text{H}(\alpha, \text{tt})\text{p}$ and ${}^3\text{H}(\alpha, \text{pt})\text{t}$ reaction mechanisms by the analysis of (E_t, E_t) and (E_p, E_t) bidimensional spectra, we used the apparatus scheme described in our previous work [1] where the target made of titanium backing (2.6 mg/cm² thick) saturated with tritium (equivalent to the thickness of about 0.15 mg/cm²) and the α -particle beam of 67.2 ± 0.4 MeV, produced by the isochronous cyclotron accelerator U-240 of the Institute for Nuclear Research at Kiev, were used.

To detect the products of the $\alpha + \text{t}$ reaction and to avoid the coincidence events related to the particles present in the above-mentioned reaction that are not of our interest, we used two $\Delta E - E$ telescopes placed to the left and, to the right of the beam direction assumed as polar axis. We used a pair of ΔE -E telescopes to detect t-t and p-t coincidences from the ${}^3\text{H}(\alpha, \text{ttp})$ reaction. The telescope placed on the right side consisted of ΔE (90 μm thick totally depleted silicon surface barrier detector (SSD)) and E [Si(Li) with 3 mm^t] detectors, while the telescope placed on the left side consisted of ΔE [400 μm SSD] and E [NaI(Tl) with 20 mm ^{ϕ} \times 20 mm^t] detectors. The calibration of the scintillator was made using the same procedure described in our previous paper [1], while a standard technique was used for the SSD. We recorded the signals coming from the two telescopes within a window time of about 100 ns by using a standard electronic set-up. The (E_t, E_t) and (E_p, E_t) bidimensional spectra were obtained by the t-t and p-t coincidence events and some results are presented in Figs. 2 (a) and 3 (a), respectively.

The corresponding experimental $Q_{3\text{exp}}$ -value distributions (see Figs. 2 (b) and 3 (b)) deduced from the considered spectra (Figs. 2 (a) and 3 (a)), by using the energy and momentum conservation laws[6], provide the opportunity of estimating the correctness of the related measurements, and of determining the total experimental error. We obtain for the t-t coincidence events the experimental Q-value peak of - 19.71 MeV for the $Q_{(\text{three-body})}$ distribution (while the theoretical Q-value is -19.81 MeV) and the FWHM value of about

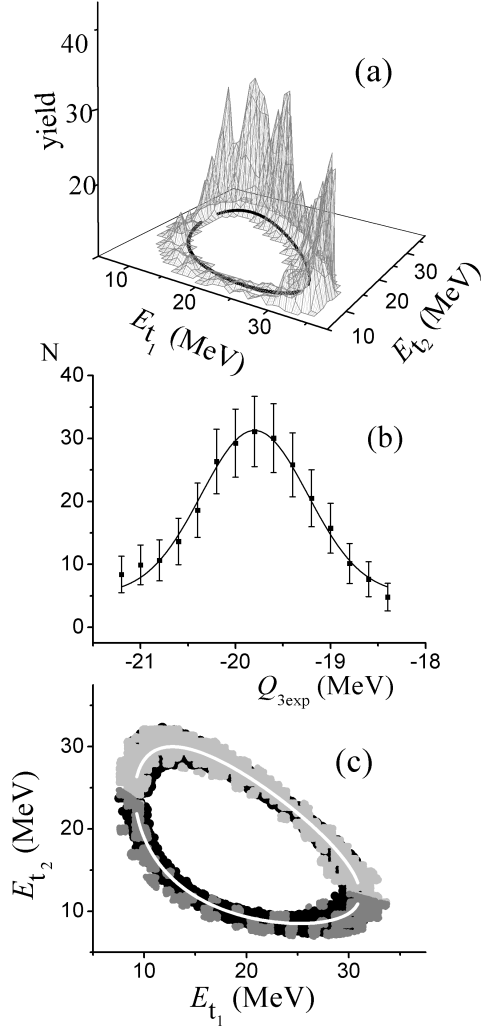


FIG. 2. (a) Experimental bidimensional spectrum of the t-t coincidence events for the ${}^3\text{H}(\alpha,tt)\text{p}$ reaction at $E_\alpha=67.2$ MeV, $\theta_1 = +20^\circ$ (right side), and $\theta_2 = -21^\circ$ (left side). Black solid lines represent kinematic curves for the corresponding experimental conditions. (b) Experimental Q-value distribution for the three-body reaction obtained by the bidimensional spectrum analysis; solid line is the result of the fit. (c) (E_{t_1}, E_{t_2}) bidimensional spectrum separated in upper (light grey) and lower (grey) branches, while a black background represents Monte Carlo kinematic calculations, and white solid lines represent kinematic calculations in the frame of a punctual geometry.

1.54 MeV (see Fig. 2 (b)) with a standard deviation σ of 0.65 MeV for the fit by a Gaussian function. In the case of p-t coincidences we obtain the value of - 19.80 MeV for the experimental Q-value peak (see Fig. 3 (b)) and the FWHM value of 1.32 MeV with a standard deviation of 0.56 MeV. Both of the $Q_{(\text{three-body})}$ experimental determinations are consistent

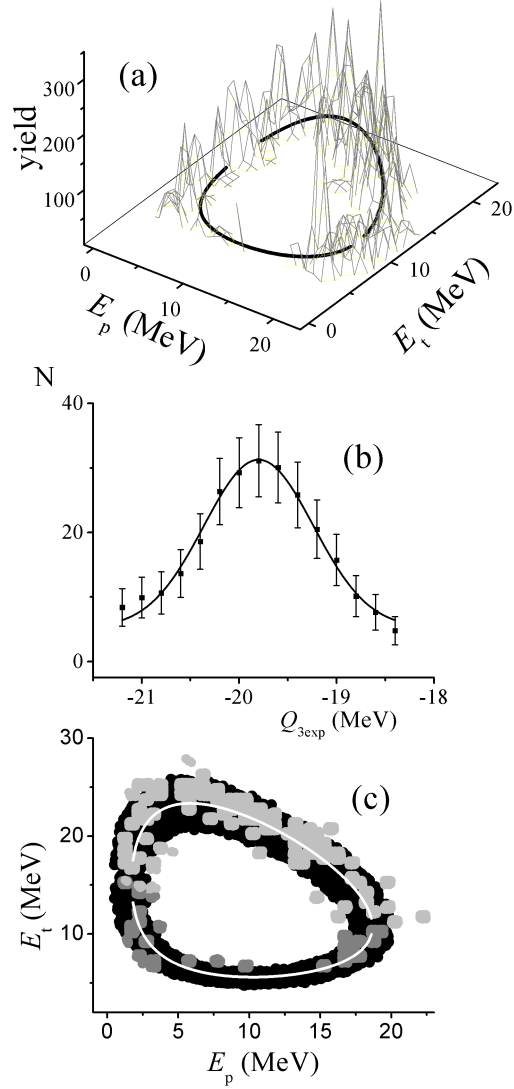


FIG. 3. As Fig. 2, but with detectors placed at $\theta_p = -27.5^\circ$ (left side) and $\theta_t = +15^\circ$ (right side) for the ${}^3\text{H}(\alpha, \text{pt})\text{t}$ reaction and the (E_p, E_t) bidimensional spectrum.

and in agreement with the theoretical three-body Q -value. These results indicate the correctness of all experimental treatment and analysis procedure in the ${}^3\text{H}(\alpha, \text{tt})\text{p}$ and ${}^3\text{H}(\alpha, \text{pt})\text{t}$ three-body experiments taking into account the detector resolution, beam resolution, energy straggling in the target, effect of differential target thickness, kinematic changing from beam spot size, and beam divergence. For a further analysis of the experimental data coming from the ${}^3\text{H}(\alpha, \text{tt})\text{p}$ and ${}^3\text{H}(\alpha, \text{pt})\text{t}$ reactions we projected the upper and lower loci of the kinematical curves on the E_t (or E_p) energy axis of tritons (or protons). As Figs. 2 (c) and 3(c) show, the (E_t, E_t) and (E_p, E_t) bidimensional spectra are separated into upper and

lower branches. By using the Monte Carlo calculation, described in [7] and previously used in the study of excited ${}^6\text{Li}$ levels by the ${}^3\text{H}(\alpha, \tau t)n$ three-body reaction [1], we reproduced the bidimensional coincidence event distribution obtained in the experiment by simulation. By projecting the event distribution as obtained in Fig. 2 on the E_{t_1} -axis for the (E_{t_1}, E_{t_2}) bidimensional spectrum, or on the E_p -axis for the (E_p, E_t) spectrum obtained in Fig. 3, we analyze the various resonance contributions.

The yield of a three-body reaction, where two-body resonances at intermediate step of the process are formed, can be calculated by a sum of the Breit-Wigner contributions

$$N \propto \rho(\Omega_{t_1}, \Omega_{t_2}, E_{t_1}) \times \left(\sum_{j=1}^n C_j \frac{(1/2\Gamma_j)^2}{(E_j - E_{pt})^2 + (1/2\Gamma_j)^2} + \sum_{l=1}^m A_l \frac{(1/2\Gamma_l)^2}{(E_l - E_{tt})^2 + (1/2\Gamma_l)^2} \right), \quad (1)$$

where ρ is the phase space factor of the three-body reaction, C_j is the corresponding contribution of each unbound ${}^4\text{He}^*$ state decaying into the p+t particles, and A_l is the corresponding contribution of each ${}^6\text{He}^*$ level decaying into the t_1+t_2 clusters. The values of relative energies and phase space factor of the sequential three-body reaction used in expression (1) are calculated by the Monte Carlo simulation taking into account the geometry and energy parameters of the experiment.

III. DATA ANALYSIS

The bidimensional spectra of the t-t and p-t coincidence events obtained by the ${}^3\text{H}(\alpha, tt)p$ and ${}^3\text{H}(\alpha, pt)t$ three-body reactions contain experimental information about the unbound excited states of ${}^6\text{He}^*$ and ${}^4\text{He}^*$ corresponding to the t+t and p+t systems, respectively. Starting from the $\alpha+{}^3\text{H}$ interaction in the entrance channel, the ways of forming the t+t+p products in the exit channel are the following:



where the (2) and (3) processes are the mechanisms in which unbound states of ${}^4\text{He}^*$ and ${}^6\text{He}^*$ are formed, respectively, and then they decay into the corresponding pairs of particles. Process (4) is the quasifree t+t scattering in which the ${}^3\text{H}$ -particle comes from the virtual decay of $\alpha \rightarrow \text{p}+\text{t}$. Process (5) is the statistical three-body break-up. The yield of each process depends on the kinematic conditions of reacting nuclei and geometric configuration of detectors. Therefore, we have to select the detector angles in order to find the optimal conditions where the ${}^6\text{He}^*$ states with the t+t cluster structure are significantly excited and the ${}^4\text{He}^*$ resonance contributions are not strongly overlapped with those of ${}^6\text{He}^*$. In fact, we have to note that in the case of detecting t-t coincidence particles we are not sure that all registered coincidence events located along the (E_1, E_2) bidimensional spectrum at θ_1 and θ_2 detector angles correspond to events of the ${}^6\text{He}^*$ excited state formation caused only by the process (3). This is because in this bidimensional spectrum t-t coincidence events caused by the process (2) where ${}^4\text{He}^*$ states are formed are also present. Therefore, when we analyze the energy spectrum (see for example Fig. 4 (b)) by projecting the coincidence events of the upper branch of the bidimensional loci onto the E_t -axis (for example, the E_t energy value registered by the detector placed at $\theta_1 = +20^\circ$), we have peaks contributed by coincidence events belonging to the ${}^6\text{He}^*$ states (formed by process (3)) and also to the ${}^4\text{He}^*$ states (formed by process (2)). In fact, if p is the spectator particle (the residual non-resonant particle at the first step of reaction) detected in our case at $\theta_p = -21^\circ$ and t (detected at $\theta_t = +15^\circ$ in Fig. 5 or $\theta_t = +20^\circ$ in Fig. 6) is one of the two t+t cluster constituting the ${}^6\text{He}^*$ resonances decaying into two tritons at the second step of reaction populating the channel (3), we can observe some resonance features of the p-t coincidence events along the kinematic loci of the (E_p, E_t) bidimensional spectrum in correspondence of some particular E_p values. In such a case, since we analyze a kinematically complete three-body reaction by the $E_p, E_t, \theta_p, \phi_p, \theta_t, \phi_t$ measurements, we are able to determine the $E_{\text{pt}}, E_{\text{tp}},$ and E_{tt} relative kinetic energies for each coincidence event. Therefore, we know what t+t excited states of ${}^6\text{He}^*$ are populated in the spectrum. On the other hand, if t is the spectator particle detected at $\theta_t(+15^\circ$ or $+20^\circ$ in Fig. 5 or 6, respectively) leaving the ${}^4\text{He}^*$ states and the p particle detected at $\theta_p = -21^\circ$ is one of the two p+t particles produced by the ${}^4\text{He}^*$ decay populating the channel (2), we know which E_{tp} relative kinetic energy values of the ${}^4\text{He}$ resonant states can enhance the coincidence event distribution along the kinematic loci of the (E_p, E_t) bidimensional spectrum. An appropriate choice of the detector

angle configuration avoids the possible strong overlap of ${}^6\text{He}^*$ and ${}^4\text{He}^*$ contributions in the p-t coincidence events. Therefore, only the inspection of the coincidence event contribution projected onto the E_p -axis of Figs. 5 and 6 in relation to the E_{pt} , E_{tp} , and E_{tt} relative kinetic energies, by using relation (1) in calculation of our analysis can allow us to individualize ${}^6\text{He}^*$ and ${}^4\text{He}^*$ resonant contributions formed by the (2) and (3) processes which are both present in the bidimensional (E_p, E_t) spectra of the p+t+t three-body reaction. We then determine the E^* and Γ width values for all ${}^6\text{He}^*$ and ${}^4\text{He}^*$ resonant contributions considered in Figs. 4 (b), 5 (b), and 6 (b) as results of the fit procedure.

Therefore, without an accurate analysis of the various resonance peaks formed by the decay of both ${}^6\text{He}^*$ and ${}^4\text{He}^*$ states that we consider in this work (taking into account the E_{tt} , E_{pt} , and E_{tp} relative energies and various resonant contributions in formula (1)), it is impossible to separate the decay contributions of the various ${}^6\text{He}^*$ states from the ones caused by the decay of the ${}^4\text{He}^*$ states, or to determine the E^* excitation energy and Γ width values of the investigated ${}^6\text{He}^*$ states in a reliable way. Of course, the choice of the angular configuration of detectors and projection of events onto the E_t - or E_p -axis in order to obtain the energy spectrum can favour the yields of some ${}^6\text{He}^*$ peaks in comparison with the ones of ${}^4\text{He}^*$ peaks, but the competition between the (2) and (3) processes and presence of both their contributions are not eliminable by any hardware or software treatment. Therefore, we need to take into account all possible ${}^6\text{He}^*$ and ${}^4\text{He}^*$ state contributions in relation (1) in the analysis.

We think it is important to investigate the existence of the 18 MeV ${}^6\text{He}^*$ energy region by analyzing the bidimensional spectra obtained by the ${}^4\text{He}+{}^3\text{H}$ reaction and to compare our results with the ones obtained by the ${}^7\text{Li}+{}^6\text{Li}$ [4] and $n+{}^7\text{Li}$ [5] experiments. In order to observe the effects of the 18 MeV ${}^6\text{He}^*$ state formation by its decay into the t+t channel we selected the angles of telescopes as $\theta_1=+20^\circ$ and $\theta_2 = -21^\circ$ in order to make the E_{tt} relative energy function very flat around the excitation energy of our interest along the bidimensional kinematic curve. This is an optimal condition to determine the E^* energy of the ${}^6\text{He}^*$ state with the best energy resolution because the flat behaviour of the E_{tt} relative energy avoids distortion effects due to the projection of coincidence events on the E_{t_1} -axis (or analogously on the E_{t_2} -axis) of the two-dimensional event distribution. However such mentioned detector geometry does not allow a better determination of the Γ width value. In fact, in order to obtain the more realistic determination of Γ width it is convenient to project

the (E_p, E_t) coincidence events on the E_p -axis, and eventually to select appropriate θ_p and θ_t detector angles so that it is possible to range a larger interval of E_{tt} relative energies around the 18 MeV ${}^6\text{He}^*$ peak energy (see Figs. 5 and 6).

In a bidimensional spectrum, the finite angular and energy resolutions of detectors contribute to the spreading of events in the (E_1, E_2) plane, where E_1 and E_2 are the energies of the two detected coincidence particles. Therefore, it should be necessary to separate the geometric effects from the energy ones before the treating of data. Since this is a very difficult task, we decided to analyze the bidimensional spectra by the Monte Carlo method as we did in a recent previous work [1]. We have generated a sufficient set of random events suitable to obtain the t-t or p-t coincidences. In the Monte Carlo simulation we take into account the value of the beam energy and its dispersion, the thickness of the target, the energy loss in the target, the size of the spot beam on the target, the target-detector distances, and the energy resolution of detectors. To analyze the experimental data obtained by the ${}^3\text{H}(\alpha, \text{ttp})$ reaction, we should project the upper and the lower loci of the kinematic curve onto the E_{t_1} energy axis (see Fig. 2) or onto the E_p energy axis (see Fig. 3). The procedure is performed by recalculating the (E_{t_1}, E_{t_2}) or (E_p, E_t) bidimensional spectra of coincidence events by using the Monte Carlo method and projecting their yields onto the E_t or E_p axis. The selected (E_{t_1}, E_{t_2}) bidimensional spectrum, obtained for the E_α beam energy of 67.2 MeV and detectors placed at $\theta_{t_1} = \theta_1 = +20^\circ$ and $\theta_{t_2} = \theta_2 = -21^\circ$ are divided into upper and lower branches (see Fig. 2) by using the above-mentioned method, and the upper branch of bidimensional loci is projected onto the E_{t_1} energy axis (see Fig. 4 (b)). Moreover, Fig. 4 (a) shows the relative kinetic energies of the t-t, p-t, and t-p pairs of particles versus E_{t_1} , where E_{t_1} is the energy value of the triton that is registered by the detector placed at $\theta_1 = +20^\circ$ while the other triton of E_{t_2} energy is registered by the detector placed at $\theta_2 = -21^\circ$. The analysis of the full resonant structures that appear in the spectrum of Fig. 4 (b) joined with the corresponding E_{tt} , E_{pt} , and E_{tp} relative kinetic energies described by the lines reported in Fig. 4 (a) allows us to know if one resonant peak of the event distribution is contributed by some ${}^6\text{He}$ excited states that decay into the t+t particles, or by some ${}^4\text{He}$ excited states that decay into p+t particles, or eventually if the peak can be formed by some overlapped contributions caused by the decay channels of ${}^6\text{He}^*$ and ${}^4\text{He}^*$ states. In the fit procedure of relation (1) we use the E^* and Γ width parameters given in Ref. [8] as starting values for the ${}^4\text{He}^*$ resonances giving the calculation procedure the possibility of adjusting such

parameters, while the values were fully free for the parameters of the ${}^6\text{He}^*$ resonances.

As Fig. 4 (a) shows, it is evident that the trend of the E_{tt} function remains almost constant with a small fluctuation around the 6.0 MeV value. Taking into account the threshold energy

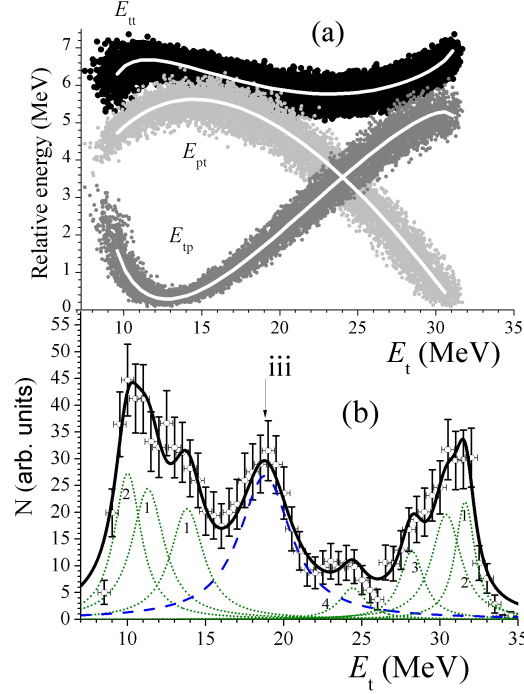


FIG. 4. (Color online) (a) The white solid lines represent the E_{tt} , E_{pt} , and E_{tp} relative kinetic energies of the outgoing particle pairs versus the E_t energy for the ${}^3\text{H}(\alpha, tt)\text{p}$ three-body reaction, at incident energy $E_\alpha = 67.2$ MeV, and with the detectors placed at $\theta_{t_1} = \theta_1 = +20^\circ$ and $\theta_{t_2} = \theta_2 = -21^\circ$. The Monte Carlo calculations are presented as colorful arrays of dots. (b) The spectrum obtained as projection of the upper branch of the t-t coincidence yields onto the E_t -axis of detector placed at θ_1 . The central peak (dashed line) labelled as iii is due to the population of the high-lying ${}^6\text{He}^*$ state at about 18 MeV of excitation energy decaying into the t+t channel. The other resonant contributions are due to the ${}^4\text{He}^*$ state formation decaying into the p+t particles. The “left” resonance structure is due to the first two ${}^4\text{He}^*$ excited states at 20.2 and 21.0 MeV (dotted lines, labelled as 1 and 2, respectively) and the “right” resonance is due to the first four ${}^4\text{He}^*$ excited states (dotted lines, labelled as 1, 2, 3 and 4) where the third and fourth excited states are at 21.8 and 23.3 MeV, respectively. The solid line is the sum of all contributions.

of 12.31 MeV for the ${}^6\text{He}^*$ level that decays into the t-t channel, the peak energy of the event distribution included in the 16-23 MeV E_t energy range corresponds to the excitation energy of 18.3 MeV for the ${}^6\text{He}^*$ nucleus. Therefore, this ${}^6\text{He}$ excited state was populated in our

${}^3\text{H}(\alpha, \text{tt})\text{p}$ experiment. Moreover, the figure shows that the set of full E_{tt} values around the considered ${}^6\text{He}^*$ level ranges within the interval of about 0.7 MeV. This means that, in respect to the behaviour of the E_{tt} shape, the energy peak is well determined with a small error of ± 0.2 MeV while the FWHM determination is affected by the small 0.7 MeV range of the E_{tt} relative energy values around the peak at 18.3 MeV of ${}^6\text{He}^*$ state. Instead, by the other analyzed energy spectra versus E_{p} corresponding to different detector angles we can determine the Γ width value of the above-mentioned ${}^6\text{He}^*$ state in a reliable way (see Figs. 5 (b) and 6(b)) because the relative energy values of the complete E_{tt} function range in an interval of about 8 MeV.

Figure 4 (b) shows the event distribution due to the projection of the upper branch of the $(E_{\text{t}_1}, E_{\text{t}_2})$ bidimensional spectrum onto the E_{t_1} energy measured by the detector placed at $\theta_1 = 20^\circ$. The error bars take into account only the statistical error, while the finite energy resolution of the used electronic system is about 0.4 MeV. As one can see, three resolved contributions appear in this figure. On the left side, in the $8 \text{ MeV} < E_{\text{t}} < 16 \text{ MeV}$ energy range, the main resonance contributions are due to the population of the first two ${}^4\text{He}$ excited states and their decay into the p+t channel (process (2)), when the first emitted t-particle (the spectator in the process (2)) goes to the detector placed at θ_1 while the t-particle coming from the decay of ${}^4\text{He}$ excited states into the p+t channel goes to the detector placed at θ_2 ; the particular trend of the E_{t} line with inversion of the relative kinetic energy value of the t+p system in Fig. 4 (a) leads to the repetition of some ${}^4\text{He}^*$ resonant state contributions at increasing E_{t} energy values along the E_{t} -axis. In the central part of the figure, in the 16-23 MeV E_{t} energy range, the main contribution is due to the 18 MeV ${}^6\text{He}^*$ state formation and to its decay into two tritons detected at θ_1 and θ_2 angles (process (3)); on the right side, in the $23 \text{ MeV} < E_{\text{t}} < 35 \text{ MeV}$ energy range, a wide complex resonant structure is due to contributions of the first four ${}^4\text{He}$ excited states which decay into the p+t channel with the first t-particle (the spectator in the process(2)) that goes to the detector placed at θ_2 while the t-particle coming from the decay of ${}^4\text{He}$ excited states into the p+t channel goes to the detector placed at θ_1 .

The final calculation result obtained by using expression (1) and the least squares method with variables describing the energy peak and width of the various contributions of the ${}^4\text{He}^*$ and ${}^6\text{He}^*$ states is reported in Fig. 4 (b) by a solid line. The dotted lines represent the single contributions Γ of the various ${}^4\text{He}^*$ levels while the dashed line represents the resonant

contribution of the 18.3 MeV ${}^6\text{He}^*$ state. The obtained values of 18.3 ± 0.2 MeV for the E^* energy peak and 0.4 ± 0.2 MeV for the Γ width regarding the mentioned ${}^6\text{He}^*$ state, labelled as iii in Fig. 4 (b), are also reported in Table I.

With the aim of checking these obtained results in the 18.3 MeV ${}^6\text{He}^*$ state and in order to extend our investigation on the other near high-lying ${}^6\text{He}^*$ states, we studied (E_p, E_t) bidimensional spectra by projecting the p-t coincidence events onto the E_p -axis with different geometric configuration of detectors and by analyzing the obtained E_p energy spectra. At first we selected the coincidence events when the proton goes to the detector placed at $\theta_p = \theta_1 = -21^\circ$ while the triton is detected at $\theta_t = \theta_2 = +15^\circ$. As Fig. 5 (a) shows, the shapes of the E_{tt} , E_{pt} , and E_{tp} relative energies of the t-t, p-t and t-p systems are very different in comparison with ones presented in Fig. 4 (a). In fact, in the case of Fig. 5 (a) it is possible to explore the E_{tt} relative energy range of about 8 MeV for the decay of ${}^6\text{He}^*$ states into the t-t channel.

Figure 5 (b) shows the energy spectrum of the event distribution obtained by projection of the upper branch of coincidence events versus the E_p energy measured by the detector placed at $\theta_p = -21^\circ$. In this E_p energy spectrum the resonance structures at $E_p < 9.5$ MeV are contributed by the first two ${}^4\text{He}^*$ states, labelled in figure as 1 and 2, while the ones at $E_p > 9.5$ MeV are contributed by the three ${}^6\text{He}^*$ levels at excitation energies included in the 13.5-19.0 MeV range. Analogously to what was observed in the description of the left part of the spectrum in Fig. 4, in the case of the $E_p < 9.5$ MeV region the contributions of the first two excited ${}^4\text{He}$ state formation are present twice at increasing E_p , due to the inversion and repetition of the E_{tp} relative kinetic energy values of the t+p system. Therefore, by using expression (1), we obtain by the least squares calculation method the values of E^* and Γ parameters for the ${}^6\text{He}^*$ states, labelled in figure and Table I as i, ii, and iii, corresponding to the ${}^6\text{He}$ excitation energies of 14.0 ± 0.4 , 15.8 ± 0.4 , and 18.5 ± 0.4 MeV with Γ width values of 0.7 ± 0.3 , 0.8 ± 0.3 , and 1.1 ± 0.4 , respectively. The present analysis of the (E_p, E_t) bidimensional spectrum confirms the population of the 18 MeV ${}^6\text{He}^*$ level found by the fit of data of Fig. 4 (b) where the peak energy of 18.3 ± 0.2 MeV was determined with a better energy resolution, while in the analysis of the energy spectrum of Fig. 5 (b) versus the E_p -axis a realistic Γ determination of 1.1 ± 0.4 MeV for the mentioned ${}^6\text{He}$ level was obtained from a spectrum where the set of values of the E_{tt} relative energies ranges in the 8 MeV interval which includes the full values describing the complete energy spectrum of the

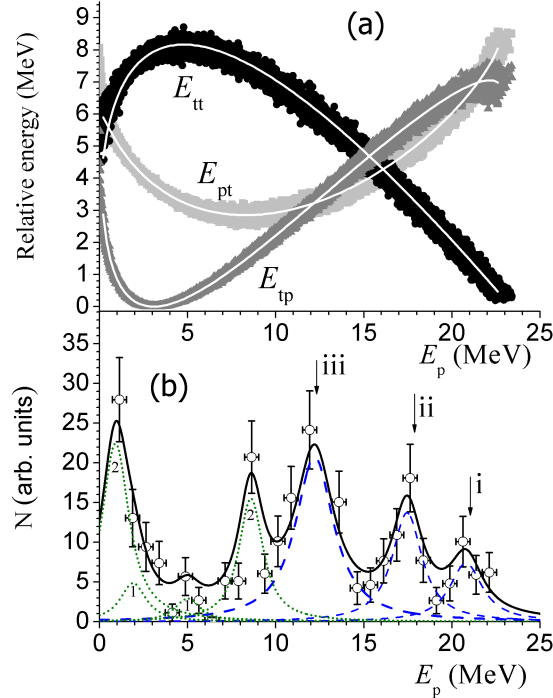


FIG. 5. (Color online)(a) The E_{tt} , E_{pt} , and E_{tp} relative energies of the outgoing particle pairs for the ${}^3\text{H}(\alpha,pt)t$ three-body reaction at $\theta_p = -21^\circ$ and $\theta_t = +15^\circ$ versus the E_p energy, calculated in the frame of a punctual geometry are indicated by white solid lines. The Monte-Carlo calculation is presented as colorful arrays of dots. (b) The spectrum obtained as projection of the upper branch of the p-t coincidence yields onto the E_p -axis. The peaks at $E_p > 9.5$ MeV labelled as i and ii (thin dashed lines), and iii (thick dashed line) are the contributions due to the population of the 14, 16 and 18 MeV ${}^6\text{He}^*$ states, respectively. The four contributions at $E_p < 9.5$ MeV labelled as 1 and 2 (dotted lines) are caused by the formation of the first two ${}^4\text{He}$ excited states at 20.2 and 21.0 MeV, respectively. The solid line is the sum of all contributions.

found 18.5 ± 0.4 MeV ${}^6\text{He}$ excited state.

Analogously to what is described in Fig. 5, in Fig. 6 we report the results of the analysis results of the (E_p, E_t) bidimensional spectrum obtained for detectors placed at $\theta_p = -21^\circ$ and $\theta_t = +20^\circ$. Figures 6 (a) and 6 (b) show results similar to the ones analyzed in Figs. 5 (a) and 5 (b), respectively. The four peaks present in the $E_p < 10$ MeV energy range are caused by the contributions of the first two excited ${}^4\text{He}$ states, as clearly appears by observing the inverse trend of the E_{tp} relative energy values around $E_p=4$ MeV of Fig. 6 (a). The three

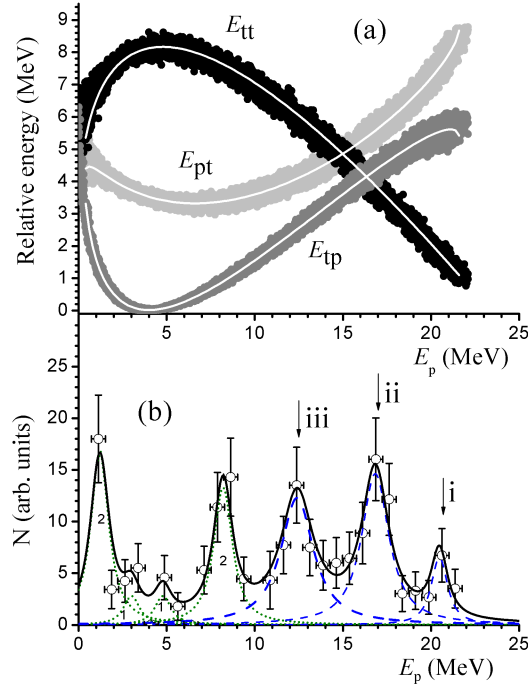


FIG. 6. (Color online) As Fig. 5, but for $\theta_t = +20^\circ$ and with the contributions of ${}^4\text{He}^*$ state formation (panel(b)) at $E_p < 10$. MeV.

peaks present in the $E_p > 10$ MeV energy range are caused by the contributions of ${}^6\text{He}^*$ states at excitation energies of 14.0 ± 0.4 , 16.1 ± 0.4 , and 18.4 ± 0.4 , respectively. The results of E^* and Γ parameters related to the ${}^6\text{He}^*$ states, labelled in Fig. 6 (b) as i, ii, and iii, are reported in Table I.

In our analysis and fit results of spectra presented in Figs. 4 (b), 5 (b), and 6 (b), for all peaks contributed by the considered ${}^4\text{He}$ excited states E^* and Γ values consistent with the ones given in literature [8] were found.

By considering the single contribution of the 18.3 MeV ${}^6\text{He}^*$ state formation obtained in Fig. 4 (b) in the analysis of the (E_t, E_t) energy spectrum, and also considering the energy distributions of the analogous ${}^6\text{He}^*$ state obtained in the analysis of the (E_p, E_t) energy spectra given in Figs. 5 (b) and 6 (b), in Fig. 7 we present the energy spectrum distribution of the mentioned ${}^6\text{He}^*$ state as a function of the E^* excitation energy of the ${}^6\text{He}$ nucleus. The full and dashed lines, corresponding to the 18 MeV ${}^6\text{He}^*$ state represented in Figs. 5 (b) and 6 (b), respectively, show the same results for the E^* energy peak and Γ width values for the investigated (E_p, E_t) bidimensional spectra; the dotted line, corresponding to the 18.3 MeV

TABLE I. E^* excitation energy and Γ width values of the ${}^6\text{He}^*$ levels for different θ_1, θ_2 geometric detector configurations, as results of the Breit-Wigner approximation by using formula(1).

| θ_1, θ_2 | Reaction | peak label | E^* (MeV) | Γ (MeV) | see Fig. |
|----------------------|---|------------|----------------|--------------------------|----------|
| +20°, -21° | ${}^3\text{H}(\alpha, \text{tt})\text{p}$ | iii | 18.3 ± 0.2 | $0.4 \pm 0.2^{\text{a}}$ | 4 (b) |
| -21°, +15° | ${}^3\text{H}(\alpha, \text{pt})\text{t}$ | i | 14.0 ± 0.4 | 0.7 ± 0.3 | 5 (b) |
| | | ii | 15.8 ± 0.4 | 0.8 ± 0.3 | ” |
| | | iii | 18.5 ± 0.4 | 1.1 ± 0.3 | ” |
| -21°, +20° | ${}^3\text{H}(\alpha, \text{pt})\text{t}$ | i | 14.0 ± 0.4 | 0.6 ± 0.4 | 6 (b) |
| | | ii | 16.1 ± 0.4 | 0.8 ± 0.4 | ” |
| | | iii | 18.4 ± 0.4 | 1.0 ± 0.4 | ” |

^a this Γ value obtained in the analysis of the energy spectrum of Fig. 4 (b) does not correspond to the true Γ width of the 18.3 MeV ${}^6\text{He}^*$ state because its determination by the (E_t, E_t) spectrum is affected by the limited accessible E_{tt} relative energy interval of about 0.7 MeV only (see Fig. 4 (a) and text for details).

${}^6\text{He}^*$ state represented in Fig. 4 (b), shows the same E^* peak value but a limited Γ width value of 0.4 MeV since it is affected by the incomplete set of the E_{tt} relative energy values reached in the analyzed (E_t, E_t) bidimensional spectrum. Therefore, the choice of using the t-t coincidence events and detector angles at +20° and -21° leads to a more reliable condition for the E^* peak determination of 18.3 ± 0.2 MeV, while its observed Γ width value of 0.4 ± 0.2 MeV is limited to cause the partial accessible E_{tt} relative energy interval of about 0.7 MeV only, instead of the 8 MeV E_{tt} interval that is explored in the analyzed spectra of the p-t coincidence events. Consequently, the Γ values are correctly determined by the analysis of the (E_p, E_t) spectra. Nevertheless, in Table I we also report the Γ width value determined by the analysis of the (E_t, E_t) bidimensional spectrum only to understand the reasons why the analysis of this spectrum leads to a smaller Γ value. In a practical way it is impossible to compare this Γ width value of 0.4 MeV extracted by the (E_t, E_t) energy spectrum of Fig. 4 (b) with the Γ width values obtained from (E_p, E_t) energy spectra of Figs. 5 (b) and 6 (b).

In literature not many results about the 18 MeV ${}^6\text{He}^*$ state with the determination of E^* and Γ parameters, and their respective errors are present. Brady *et al.* [5] in the ${}^7\text{Li}(n,$

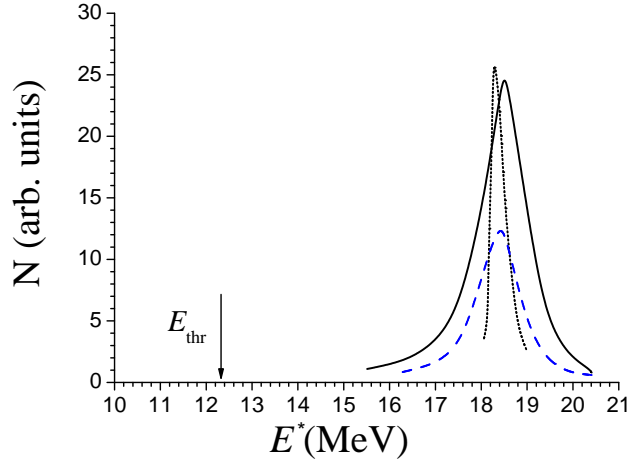


FIG. 7. (Color online) Energy spectrum distribution of the 18.3 MeV ${}^6\text{He}$ level as a function of the E^* excitation energy of the ${}^6\text{He}$ nucleus. Dotted line is obtained from the ${}^6\text{He}^*$ peak contribution around the energy interval centered at $E_t = 18.8$ MeV of Fig. 4 (b); full line is obtained from the ${}^6\text{He}^*$ peak contribution centered at $E_p = 12.2$ MeV of Fig. 5 (b); dashed line is obtained from the peak at $E_p = 12.4$ MeV of Fig. 6 (b). The arrow indicates the threshold energy of 12.31 MeV for ${}^6\text{He}^*$ decaying into the t+t channel.

d) ${}^6\text{He}$ experiment at $E_n = 56.3$ MeV observed (beside the ground state and the 1.8 MeV ${}^6\text{He}^*$ excited state) a group of at least three excited states centered near 13.6, 15.4 and 17.7 MeV by the analysis of deuteron angular distributions. However, due to poor resolution, limited statistical accuracy, uncertainty in the energy width of these states, the authors combined these three experimental states as a single broad peak centered at 15.6 MeV. Moreover, Yamagata, Akimune *et al.* [4] found in their ${}^6\text{Li}({}^7\text{Li}, {}^7\text{Be t}){}^3\text{H}$ experiment, at $E_{7\text{Li}}=455$ MeV by the analysis of the t-particle single spectra, the resonance of ${}^6\text{He}^*$ state decaying into the t+t clusters at $E^* = 18 \pm 1$ MeV with a Γ width of 9.5 ± 1 MeV (see Fig. 3 (c) of Ref. [4]).

We believe that in the analyzed single spectra of Ref. [5] it was impossible to solve the various resonance contributions of excited states present in the region of ${}^6\text{He}$ levels included in the range between the threshold energy of 12.31 MeV for the decay into the t+t channel and the excitation energy of about 22 MeV.

Also in the Akimune *et al.* [9] and Yamagata *et al.*'s experiments [4], by the analysis of

the t-particle single spectra, it was impossible to solve the true t-t resonant contribution of the ${}^6\text{He}$ excited state at about $E^* = 18$ MeV due to the various high-lying ${}^6\text{He}$ levels populated by channel (3) from the contributions caused by channel (2). This is where the first t-particle leaves the various ${}^4\text{He}^*$ state formations while the second t-particle comes from the decay of ${}^4\text{He}^*$ into the p+t system. In addition, the background contribution of the t-particles caused by the (4) and (5) channels is also present in the collected spectrum. Therefore, the resulting analyzed spectrum of the authors [4, 9] appears as a convolution of the various resonant contributions caused by the (2) and (3) channels in addition to the non resonant background due to the (4) and (5) channels. Instead, in the analysis of the (E_t, E_t) and (E_p, E_t) bidimensional spectra of our ${}^3\text{H}(\alpha, \text{ttp})$ kinematically complete experiment, it was possible to separate and observe the population of the 18.3 MeV ${}^6\text{He}^*$ state from the other resonant contributions and also to find reliable Γ width values for the mentioned ${}^6\text{He}^*$ state. Moreover, we also found the Γ width values of $0.6 \pm 0.4 - 0.7 \pm 0.3$ MeV for the 14.0 ± 0.4 MeV ${}^6\text{He}^*$ state and 0.8 ± 0.4 MeV for the 16.1 ± 0.4 MeV ${}^6\text{He}^*$ state. These last Γ width determinations for the 14.0 and 16.1 MeV ${}^6\text{He}^*$ states are new findings because such found values are completely different from the ones reported in compilations [2, 3].

IV. CONCLUSIONS

In our described ${}^4\text{He}+{}^3\text{H}$ experiment, at E_α beam energy of 67.2 MeV, the ${}^6\text{He}^*$ level at 18.3 ± 0.2 MeV was populated. This level shows the Γ width of 1.1 ± 0.4 MeV by its decay into the binary t+t channel. These results have been obtained by analyzing the (E_t, E_t) and (E_p, E_t) bidimensional spectra at various detector geometry angles by reactions leading to the p+t+t three-body system through the (2) and (3) processes where ${}^4\text{He}^*$ and ${}^6\text{He}^*$ resonant states are formed, respectively. The study shows resonant contributions due to the population of high-lying ${}^6\text{He}^*$ levels by projecting the coincidence events either onto the E_t -axis or onto the E_p -axis. In both cases, the observed peaks in the energy spectra of coincidence events confirm the population of the ${}^6\text{He}^*$ state at E^* of 18.3 MeV by the analysis of the E_{tt} relative energies of coincidence events (see Figs. 4 (b), 5 (b), and 6 (b)). In the considered energy spectra peaks formed by the coincidence events are also present due to the decay of the ${}^4\text{He}^*$ state formation into the p+t channel by the analysis of the E_{pt} and E_{tp} relative energies. The reliability of the analysis of spectra and results obtained in

our experiment is confirmed by the experimental Q -value distributions shown in Figs. 2 (b) and 3 (b), by the clear evidence of both contributions of ${}^6\text{He}^*$ and ${}^4\text{He}^*$ states in Figs. 4 (b), 5 (b) and 6 (b), and by the complete consistent results shown in Fig. 7 and Table I. In the present experiment we also observed the population of two other ${}^6\text{He}^*$ states at excitation energy E^* at 14.0 and 16.1 MeV. The E^* energy peak values are in agreement with the ones reported in [2] and [3]. On the contrary, the found Γ width values are strongly different from the ones reported in the above mentioned compilations. We also compared our E^* and Γ results about the 18.3 MeV ${}^6\text{He}^*$ state with the ones obtained by Yamagata *et al.* [4], Akimune *et al.* [9], and Brady *et al.* [5] in their experiments by the ${}^6\text{Li}({}^7\text{Li}, {}^6\text{He}){}^7\text{Be}$ [4, 9] and ${}^7\text{Li}(n, d){}^6\text{He}$ [5] reactions, and discussed the relevant difference in the Γ width value determinations.

The choice of the beam energy, detector geometry, and kind of reaction allowed us to measure the peak energy of the high-lying 18.3 MeV ${}^6\text{He}^*$ level with the precision of 0.2 and 0.4 MeV in the energy spectra of the ${}^3\text{H}(\alpha, tt)p$ and ${}^3\text{H}(\alpha, pt)t$ reactions, respectively, where for this level the Γ width determinations were 1.1 ± 0.3 and 1.0 ± 0.4 MeV (see Fig. 7 and Table I) by the two analyzed (E_p, E_t) energy spectra. Moreover, we explained the reasons which led to some relevant differences among the results of the investigated reactions, since in each observed (E_t, E_t) or (E_p, E_t) energy spectrum both contributions of ${}^6\text{He}^*$ and ${}^4\text{He}^*$ excited states are present. Moreover, we also found realistic Γ width values of about 0.7 ± 0.3 and 0.8 ± 0.3 MeV for the 14.0 and 16.1 MeV ${}^6\text{He}^*$ levels, respectively.

ACKNOWLEDGMENTS

The authors wish to thank the staff of the Institute for Nuclear Research Laboratories (Kiev) for their help during the measurements. This work was supported by INR of the Academy of Sciences of Ukraine, and partially by the Istituto Nazionale di Fisica Nucleare of Italy.

-
- [1] O. Povoroznyk, O. K. Gorpinich, O. O. Jachmejov, H. V. Mokhnach, O. Ponkratenko, G. Mandaglio, F. Curciarello, V. D. Leo, G. Fazio, and G. Giardina, J. Phys. Soc. Jpn. **80**, 094204 (2011).

- [2] F. Ajzenberg-Selove, Nucl. Phys. A **490**, 1 (1988).
- [3] D. Tilley, C. Cheves, J. Godwin, G. Hale, H. Hofmann, J. Kelley, C. Sheu, and H. Weller, Nucl. Phys. A **708**, 3 (2002).
- [4] T. Yamagata *et al.*, Phys. Rev. C **71**, 064316 (2005).
- [5] F. Brady, N. King, B. Bonner, M. McNaughton, J. Wang, and W. William, Phys. Rev. C **16**, 31 (1977).
- [6] W. D. M. Rae, A. J. Cole, B. G. Harvey, and R. G. Stokstad, Phys. Rev. C **30**, 158 (1984).
- [7] O. Povoroznyk, Nuclear Physics and Atomic Energy **8**, 131 (2007), in Ukrainian.
- [8] D. Tilley, H. Weller, and G. Hale, Nucl. Phys. A **541**, 1 (1992).
- [9] H. Akimune *et al.*, Phys. Rev. C **67**, 051302(R) (2003).